## Title

Treatment of Triple-Negative Breast Cancer with TORC1/2 Inhibitors Sustains a Drug-Resistant and Notch-Dependent Cancer Stem Cell Population



## Journal

Cancer Research, 76(2)

## ISSN

0008-5472

## Authors

Bhola, Neil E
Jansen, Valerie M
Koch, James P
et al.

## Publication Date

2016-01-15

## DOI

10.1158/0008-5472.can-15-1640-t

Peer reviewed

Cancer Research

# Treatment of Triple-Negative Breast Cancer with TORC1/2 Inhibitors Sustains a Drug-Resistant and Notch-Dependent Cancer Stem Cell Population

Neil E. Bhola[1], Valerie M. Jansen[1], James P. Koch[1], Hua Li[2], Luigi Formisano[1], Janice A. Williams[3], Jennifer R. Grandis[2], and Carlos L. Arteaga[1,4,5]

## Abstract

Approximately 30% of triple-negative breast cancers (TNBC) harbor molecular alterations in PI3K/mTOR signaling, but therapeutic inhibition of this pathway has not been effective. We hypothesized that intrinsic resistance to TORC1/2 inhibition is driven by cancer stem cell (CSC)-like populations that could be targeted to enhance the antitumor action of these drugs. Therefore, we investigated the molecular mechanisms by which PI3K/mTOR inhibitors affect the stem-like properties of TNBC cells. Treatment of established TNBC cell lines with a PI3K/mTOR inhibitor or a TORC1/2 inhibitor increased the expression of CSC markers and mammosphere formation. A CSC-specific PCR array revealed that inhibition of TORC1/2 increased FGF1 and Notch1 expression. Notch1 activity was also induced in TNBC cells treated with TORC1/2 inhibitors and associated with increased mitochondrial metabolism and FGFR1 signaling. Notably, genetic and pharmacologic blockade of Notch1 abrogated the increase in CSC markers, mammosphere formation, and *in vivo* tumor-initiating capacity induced by TORC1/2 inhibition. These results suggest that targeting the FGFR–mitochondrial metabolism–Notch1 axis prevents resistance to TORC1/2 inhibitors by eradicating drug-resistant CSCs in TNBC, and may thus represent an attractive therapeutic strategy to improve drug responsiveness and efficacy. *Cancer Res; 76(2); 440–52. ©2015 AACR.*

## Introduction

Triple-negative breast cancer (TNBC) accounts for approximately 15% of all breast cancers and is considered the most virulent clinical subtype of this neoplasm. Most of these tumors exhibit a basal-like gene expression signature (1). Patients with metastatic TNBC respond transiently to chemotherapy but almost invariably progress and exhibit a poor prognosis (2). Currently there are no approved targeted therapies in TNBC, underscoring the need to identify pathogenic pathways in this breast cancer subtype. Genomic and proteomic studies have identified PI3K/Akt/mTOR pathway alterations in the basal-like subtype of breast cancer, of which, approximately 80% are TNBC (3–6). However, therapeutic blockade of this pathway with single-agent inhibitors has not been effective.

Mammalian target of rapamycin (MTOR) signals via two different complexes, TORC1 and TORC2 (7). TORC1 phosphorylates S6K and 4EBP1, signal transducers involved in RNA translation and protein synthesis, while TORC2 phosphorylates and activates Akt, a major effector of PI3K signaling (8). Inhibitors of PI3K/mTOR, TORC1/2 and TORC1, are currently being developed in breast cancer patients (9). Preclinical studies using patient-derived and cell line–generated TNBC xenografts suggest an antitumor effect of PI3K/mTOR (4) and mTOR inhibitors (10). However, clinical efficacy of these drugs in patients with TNBC has been limited.

Recent publications have implicated various mechanisms of resistance to PI3K/mTOR inhibitors, such as BEZ235. These mechanisms included activation of JAK2/STAT5, STAT3, and eiF4E in various tumor models (11, 12). The PI3K/mTOR inhibitor BEZ235 binds to the kinase domain of mTOR, thus potently inhibiting both TORC1 and TORC2 complexes in addition to PI3K (13, 14). Cancer stem cells (CSC) are a subpopulation of drug-resistant cells with self-renewing and tumor-initiating capacities (15, 16). Based on these concepts, we first identified that resistance to BEZ235 was driven more by TORC1/2 inhibition than PI3K inhibition and, second, we asked whether this resistance was due to the survival of a CSC-like population. We hypothesized that TORC1/2 inhibition promotes the survival of CSCs and, therefore, targeting molecular pathways utilized by these CSCs should enhance the antitumor effect of these inhibitors against TNBC cells. We show herein that TORC1/2 inhibition results in activation of Notch 1, which, in turn, increases CSCs. Further, we show that Notch1 activation is dependent on FGFR1 and mitochondrial activity. These results point to an intrinsic limitation of TORC1/2 inhibitors in TNBC but also suggest that combinations of TORC1/2 inhibitors with antagonists of the FGFR–mitochondrial metabolism–Notch1 axis are worthy of clinical investigation in appropriately selected tumors.

[1]Department of Medicine, Vanderbilt University, Nashville, Tennessee. [2]Department of Otolaryngology, University of Pittsburgh Medical Center, Pittsburgh, Pennsylvania. [3]Cell Imaging Shared Resource, Vanderbilt University, Nashville, Tennessee. [4]Department of Cancer Biology, Vanderbilt University, Nashville, Tennessee. [5]Breast Cancer Research Program, Vanderbilt-Ingram Cancer Center, Vanderbilt University, Nashville, Tennessee.

**Note:** Supplementary data for this article are available at Cancer Research Online (http://cancerres.aacrjournals.org/).

**Corresponding Author:** Carlos L. Arteaga, Division of Hematology-Oncology, VUMC, 2220 Pierce Avenue, 777 PRB, Nashville, TN 37232. Phone: 615-936-0975; Fax: 615-343-7602; E-mail: carlos.arteaga@vanderbilt.edu

**doi:** 10.1158/0008-5472.CAN-15-1640-T

## Materials and Methods

### Cell lines and reagents

All cell lines were obtained from the ATCC and cultured according to the instructions provided by ATCC for no longer than 6 months. Cell lines were tested and authenticated by short tandem repeat (STR) profiling by the ATCC. The human Notch1 intracellular domain (hNICD) construct was a gift from Linzhao Cheng , Johns Hopkins University School of Medicine, Baltimore, MD (Addgene plasmid #17626; ref. 17). RBP-Jk *firefly* luciferase lentiviral particles were obtained from Sigma-Aldrich. The 4X-CSL luciferase plasmid was a kind gift from Raphael Kopan, Washington University School of Medicine, St. Louis, MO (Addgene plasmid #41726; ref. 18). BEZ235, MLN128, RAD001 (everolimus), and GSI-IX were obtained from SelleckChem. Lucitanib was provided by Clovis Oncology. Paclitaxel and oligomycin A were obtained from Sigma-Aldrich. The Hes1 *firefly* luciferase plasmid was a kind gift from Scott Hiebert (Vanderbilt University, Nashville, TN).

### Viability assays

Cells were seeded in 96-well black plates and treated with inhibitors or siRNAs. At variable time points, 10 μL of Alamar Blue reagent was added to each well. Plates were incubated at 37°C for 4 hours in the dark. After 4 hours, the plates were read in a GloMax Multi Detection plate reader.

### Flow cytometry of stem cell markers

The ALDEFLUOR assay (Stemcell Technologies) was performed according to the manufacturer's guidelines to identify cells with high ALDH activity. Cells were passed through a 35-μm filter, suspended in Aldefluor assay buffer + BODIPY-aminoacetaldehyde (BAAA) and incubated for 45 minutes at 37°C in the presence or absence of the ALDH inhibitor diethylaminobenzaldehyde (DEAB). CD44-APC (BD Biosciences), PROCR-PE (BD Biosciences), ESA-FITC (BD Biosciences), CD24-PE (BD Biosciences), and CD133-APC (Biolegend) antibodies were incubated with single cells in PBS/1% FβS for 30 minutes at 4°C. Cells were stained with propidium iodide (PI) or 7-AAD to exclude nonviable cells. For experiments using cells transfected with GFP-tagged hNICD, CD44-APC was used to detect the CSCs. GFP analysis by FACS analysis was used to verify transfection of the hNICD construct. The CSC markers representing tumor-initiating populations in the cell lines used and their respective references are given in Table 1.

### Mammosphere assay

Single-cell suspensions were seeded in 6-well ultra-low attachment plates (Corning) in serum-free DMEM/F12 containing 20 ng/mL EGF (R&D Systems) and 1× B27 (Life Technologies). Fresh mammosphere media were added every 3 days. Mammosphere number and volume were determined using the GelCount mammalian cell colony counter (Oxford Optronix). For microscopic images of mammospheres the original magnification of the images is × 40 (4 × 10×). For generation of secondary mammospheres, primary mammospheres were enzymatically (0.05% Trypsin) and mechanically digested by pipette tituration, imaged to assess dissociated single cells, counted and re-seeded in mammosphere media.

**Table 1.** CSC markers that represent tumor-initiating populations in the cell lines investigated

| Cell line | CSC markers for FACS analysis | Reference |
|---|---|---|
| SUM159 | $ALDH^+$; CD44hi | (36, 37) |
| BT549 | CD44hi/$PROCR^+$ | (38, 39) |
| MDA231 | $PROCR^+/ESA^+$ | (38) |
| MDA468 | CD44hi/CD24lo | (40) |
| NCI/ADR-RES | $ALDH^+$; $CD133^+/ALDH^+$ | (41) |

### Immunoblot analysis

Cell monolayers were washed and then lysed with RIPA lysis buffer (150 mmol/L Tris, pH 7.4, 100 mmol/L NaF, 120 mmol/L NaCl, 100 μmol/L sodium vanadate, and 1× protease inhibitor cocktail; Roche). Lysates (40 μg) were resolved by SDS-PAGE and transferred to nitrocellulose membranes; these were first incubated with primary antibodies at 4°C overnight or at room temperature for 2 hours followed by incubation with HRP-conjugated anti-rabbit and anti-mouse secondary antibodies (Santa Cruz Biotechnology) for 1 hour at room temperature. Immunoreactive bands were visualized by enhanced chemiluminescence (Thermo Scientific). All antibodies were from Cell Signaling Technology with the exception of FGFR1, which was obtained from Abcam.

### RNA interference

Cells were seeded in 6-well plates or 10-cm dishes. The following day, cells were transfected with siRNA oligonucleotides mixed with Lipofectamine RNAiMax (Life Technologies). Notch1, TFAM, JAG1, Rictor, and Raptor siRNA oligonucleotides were obtained from Dharmacon. FRS2 and FGFR1 siRNA was obtained from Ambion.

### Dye exclusion assay

Cells were grown in monolayer up to 70% to 80% confluence, treated with 10 μmol/L Cell Tracker Green dye (Life Technologies), and incubated in serum-free media for 30 minutes at 37°C, after which media were replaced with regular growth media for additional 45 minutes. Cells were then trypsinized and seeded at 20% confluence. Cells were analyzed by FACS on days 1 and 10 for FITC expression.

### Quantitative real-time PCR

RNA was harvested using the RNAeasy Kit (Qiagen) and used to synthesize cDNA (iSCRIPT cDNA synthesis kit, Bio-Rad) according to the manufacturer's instructions. PCR reactions were performed using SYBR Green Master Mix (Bio-Rad) and the Bio-Rad IQ5 cycler. Relative mRNA levels were standardized to GAPDH mRNA levels. The Stem Cell, Cancer Stem Cell, and Mitochondrial Metabolism PCR Arrays (SA Biosciences), containing primers for 84 pathway-specific genes each, were performed according to the manufacturer's instructions. Gene expression was verified in cells independently using primers from SA Biosciences.

### Nanostring analysis

RNA was extracted from formalin-fixed paraffin-embedded blocks of tumor biopsies obtained from patients before and after neoadjuvant chemotherapy. Nanostring Analysis was performed as previously described (19).

### Luciferase reporter assays

Cells were transiently transfected for 5 hours with the RBP-Jk, 4X-CSL or Hes1 *firefly* luciferase reporter (SA Biosciences), each

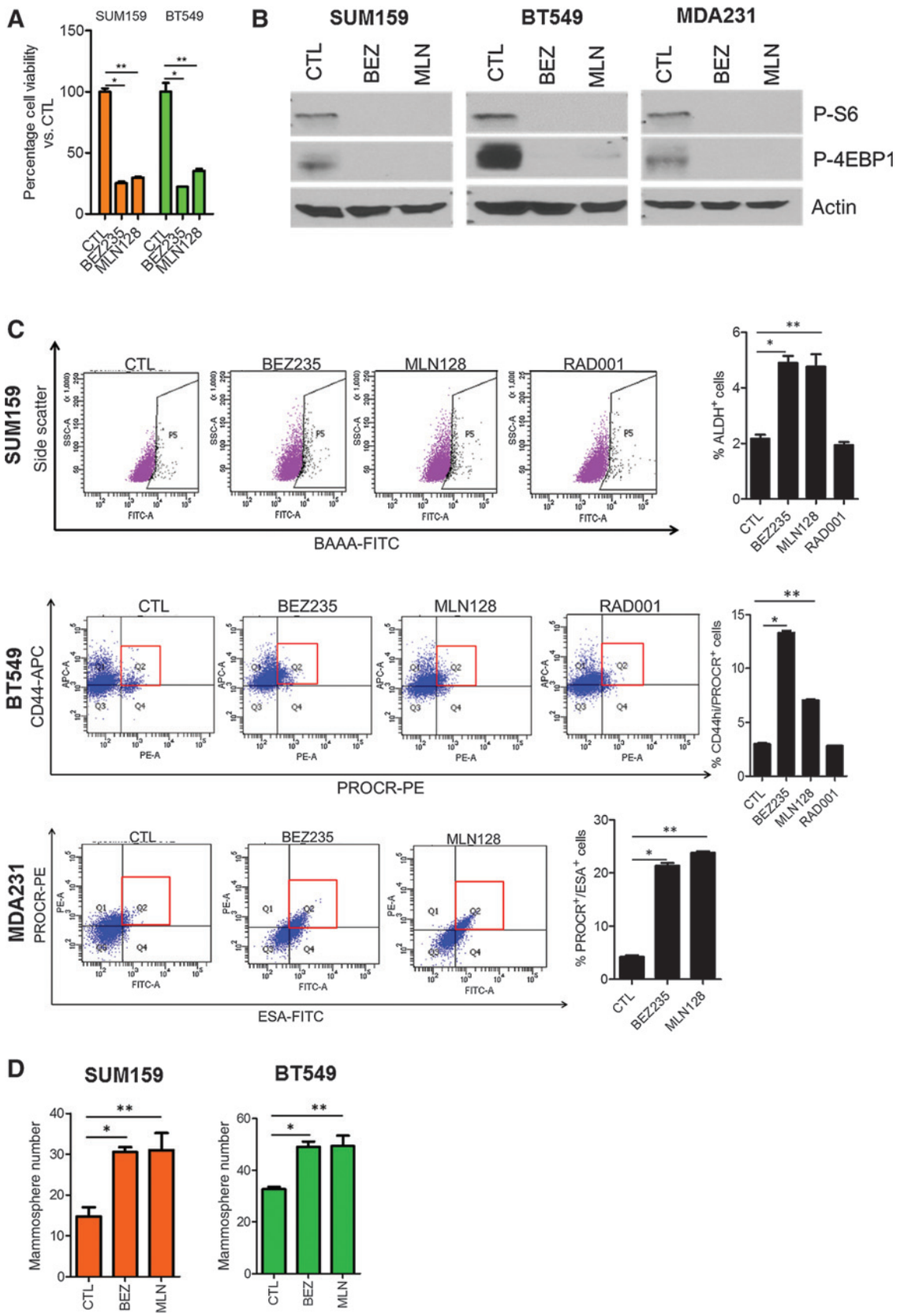
A
SUM159
BT549
Percentage cell viability vs. CTL
CTL
BEZ235
MLN128
B
SUM159
BT549
MDA231
CTL
BEZ
MLN
P-S6
P-4EBP1
Actin
C
SUM159
Side scatter
CTL
BEZ235
MLN128
RAD001
BAAA-FITC
% ALDH+ cells
BT549
CD44-APC
PROCR-PE
% CD44hi/PROCR+ cells
MDA231
PROCR-PE
ESA-FITC
% PROCR+/ESA+ cells
D
SUM159
BT549
Mammosphere number
CTL
BEZ
MLN

with a CMV *Renilla* luciferase reporter. Media were changed and cells were treated with BEZ235 or MLN128 for 17 to 48 hours. Cells were lysed and the Dual Luciferase Reporter Assay (Promega) was performed according to the manufacturer's instructions. Luciferase readings were determined using the Glo-Max Multidetection System (Promega), and the ratio of firefly luciferase to *Renilla* luciferase was calculated.

### Transmission electron microscopy

SUM159 cells were treated with vehicle, 250 nmol/L BEZ235, or 100 nmol/L MLN128 for 48 hours, processed for transmission electron microscopy (TEM) and imaged in the Vanderbilt Cell Imaging Shared Resource-Research Electron Microscopy facility.

***Embedding.*** Samples were fixed in 2.5% gluteraldehyde in 0.1 mol/L cacodylate buffer, pH 7.4 at room temperature for 1 hour and then transferred to 4°C overnight. Samples were next washed in 0.1 mol/L cacodylate buffer and incubated for 1 hour in 1% osmium tetraoxide at room temperature, followed by another wash with 0.1 mol/L cacodylate buffer. Subsequently, the samples were dehydrated through a graded ethanol series and three exchanges with 100% ethanol, followed by two exchanges with pure propylene oxide (PO). Samples were then serially infiltrated with 25% Epon 812 resin and 75% PO (1:3) for 30 minutes at room temperature, with 50% Epon 812 resin and 50% PO (1:1) for 1 hour at room temperature, and then infiltrated once more with 50% Epon 812 resin and 50% PO (1:1) overnight at room temperature. The samples were subsequently infiltrated with 100% Epon 812 resin for 48 hours and then allowed to polymerize at 60°C for an additional 48 hours.

***Sectioning and Imaging.*** Thick sections (500 nm to 1 μm) of the embedded samples were collected using a Leica Ultracut microtome. Sections were contrast stained with 1% toluidine blue and imaged with a Nikon AZ100 microscope. Ultra-thin sections (70–80 nm) were cut and collected on 300-mesh copper grids and post-stained with 2% uranyl acetate and then with Reynold's lead citrate. Samples were imaged on the Philips/FEI Tecnai T12 electron microscope at various magnifications.

### *In vivo* studies

All animal experiments and procedures were done in accordance with a protocol approved by the Vanderbilt University Institutional Animal Care and Use Committee. Athymic female mice (Harlan Sprague Dawley) were inoculated with $5 \times 10^6$ SUM159 or $8 \times 10^6$ MDA468 cells mixed with Matrigel (1:1) in the #4 mammary gland. Ten days (for SUM159) or 3 weeks (for MDA468) later, mice bearing tumors measuring $\geq$75 $mm^3$ were randomized to treatment with vehicle, MLN128 (1 mg/kg 3 times weekly p.o.), GSI-IX (10 mg/kg, 3 days on, 4 days off, i.p), or both drugs. Tumor diameters were serially measured with calipers and mouse weight determined 2 times weekly. Tumor volume in $mm^3$ was calculated by the formula: volume = length/2 $\times$ width$^2$.

### Xenograft dissociation

Xenografts were collected and tumor fragments either flash frozen in liquid $N_2$ or fixed in 10% formalin followed by embedding in paraffin. In some cases, xenografts were harvested and rinsed in PBS, mechanically minced with sterile blades in DMEM/F12/5% FBS and antibiotics/antimycotics in C-tubes (Miltenyi Biotech), and then incubated with 1× Collagenase/Hyaluronidase + 0.2 mg/mL DNAseI for 30 minutes at 37°C. Dissociated cells were passed through 70- and 35-μm filters and separated from debris using a Ficoll-Paque gradient. Cell viability was verified by trypan blue exclusion before inoculation into tumor-free nude mice.

### Statistical analysis

Statistical differences were determined using the Student *t* test. For the NanoString analysis of RNA from paired tumor biopsies, paired *t* tests were utilized. For animal studies, the differences between treatment groups were determined by the Mann–Whitney test with Bonferroni *post hoc* corrections. For the *in vivo* limiting dilution assay, extreme limiting dilution assay (ELDA) analysis was performed, and the difference between groups was recorded as described previously (20). A $P$ value of <0.05 was considered to be statistically significant.

## Results

### TNBC cell lines display CSC properties following inhibition of TORC1/2

Treatment of SUM159, BT549, and MDA231 TNBC cells with each the PI3K/mTOR inhibitor BEZ235 and the TORC1/2 inhibitor MLN128 decreased growth and expression of activated mTOR substrates S6 ribosomal protein and 4EBP-1 (Fig. 1A and B). Following a 3-day treatment with BEZ235 and MLN128 but not with the TORC1 inhibitor RAD001, surviving SUM159, BT549, and MDA231 cells were enriched for the following CSC markers as determined by FACS: ALDH$^+$, CD44hi/PROCR$^+$, and PROCR$^+$/ESA$^+$, respectively (Fig. 1C). These are established markers of tumor-initiating populations in these cell lines (Table 1). Consistent with the induced changes in CSC markers, cells surviving BEZ235 and MLN128 treatment exhibited increased mammosphere formation (Fig. 1D). Treatment with the pan-PI3K inhibitor BKM120 did not increase CSC markers in SUM159 and BT549 cells (Supplementary Fig. S1A). This result coupled with the effects induced by BEZ235 and MLN128 suggested that TORC1/2 inhibition but not PI3K inhibition was causally associated with CSC induction. Another feature of CSCs and tumor-initiating cells is increased nuclear dye/label retention (21, 22). Using a dye retention assay, we observed that 40% and 20% of cells treated 10 days with

**Figure 1.**
PI3K/mTOR and TORC1/2 inhibitors enrich for a CSC population in TNBC cell lines. A, SUM159 and BT549 cells were treated with 250 nmol/L BEZ235 or 100 nmol/L MLN128 for 72 hours. Cell viability was determined by the Alamar Blue viability assay (*, $P < 0.009$; **, $P < 0.02$). B, SUM159, BT549, and MDA231 cells treated for 72 hours were analyzed for phosphorylated S6 and 4EBP1 by immunoblot analysis. C, SUM159, BT549, and MDA231 cells were treated with 250 nmol/L BEZ235, 100 nmol/L MLN128, or 100 nmol/L RAD001 for 72 hours. FACS analysis for CSC markers (SUM159-ALDH$^+$, BT549-CD44hi/PROCR$^+$, MDA231-PROCR$^+$/ESA$^+$) was performed. Propidium iodide or 7-AAD exclusion was used to select viable cells for analysis (*, $P < 0.002$; **, $P < 0.03$). D, SUM159 and BT549 cells were treated with BEZ235 or MLN128 for 72 hours and seeded in ultra-low adherent plates as mammospheres. Mammosphere number was determined after 10 days using GelCount (SUM159: *, $P = 0.002$; **, $P = 0.02$; BT549: *, $P = 0.007$; **, $P = 0.048$). Error bars, mean ± SEM.

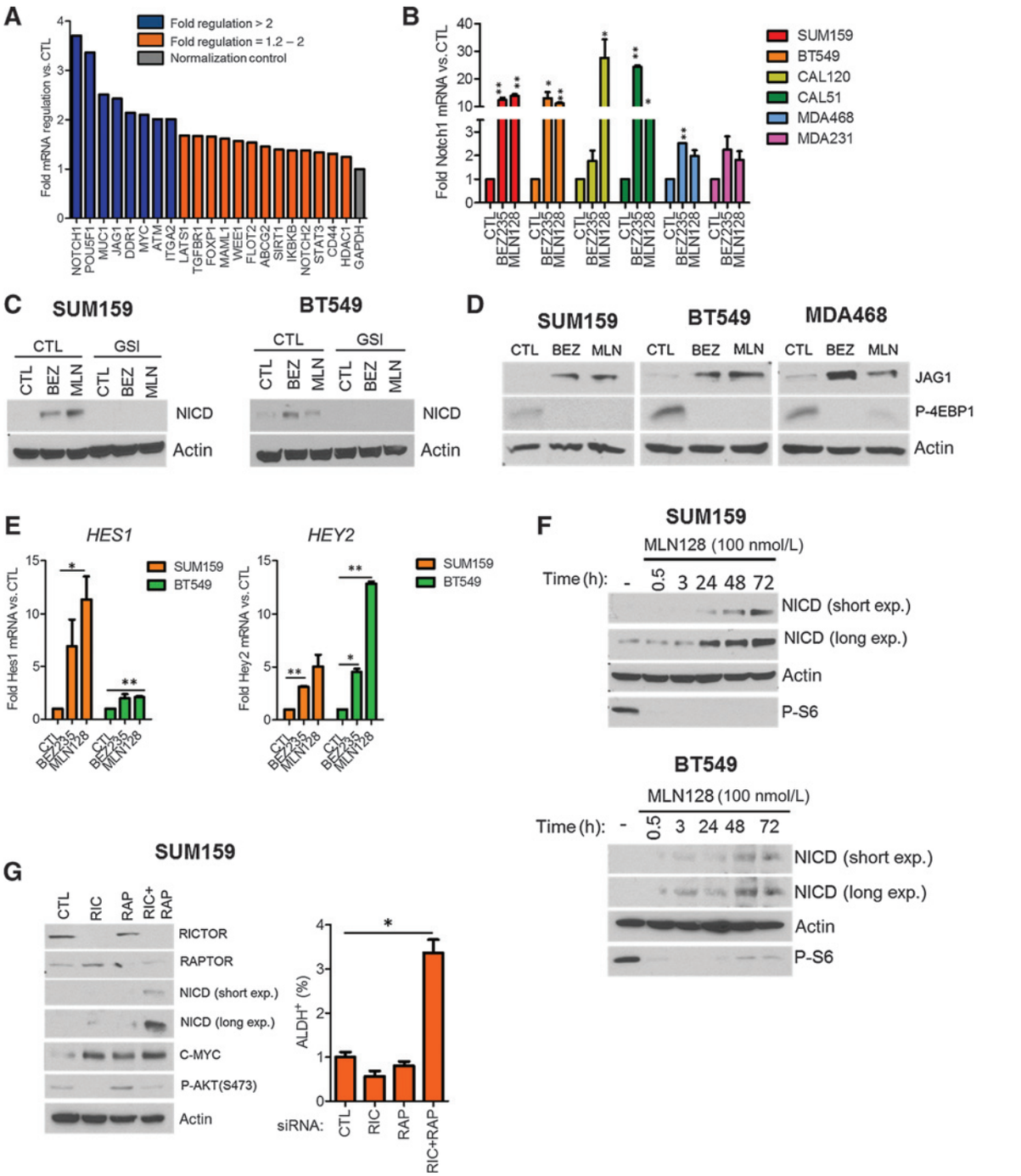


**Figure 2.**
TORC1/2 inhibition increases Notch1 expression and activity in TNBC cell lines. A, SUM159 cells were treated with control or 100 nmol/L MLN128 for 48 hours. RNA was extracted and used in the cancer stem cell–specific PCR array. Fold regulation of gene expression changes in MLN128-treated cells versus CTL was determined using the SA Biosciences PCR Array software. B, SUM159, BT549, CAL120, CAL51, MDA468, and MDA231 cells were treated with 250 nmol/L BEZ235 or 100 nmol/L MLN128 for 72 hours. q-PCR analysis was performed for *NOTCH1* (*, $P < 0.05$; **, $P < 0.005$). C, SUM159 and BT549 cells were treated with 250 nmol/L BEZ235 and 100 nmol/L MLN128 in the presence and absence of 10 μmol/L GSI-IX for 72 hours. Immunoblot analysis for the intracellular domain of Notch1 (NICD) and actin was performed. D, SUM159, BT549, and MDA468 cells were treated with 250 nmol/L BEZ235 and 100 nmol/L MLN128 for 72 hours. Immunoblot analysis for Jagged1 (JAG1), phospho-4EBP1, and actin expression was performed. E, q-PCR for Notch1 targets *HES1* and *HEY2* was performed for SUM159 and BT549 cells treated with BEZ235 and MLN128 (*, $P < 0.04$; **, $P < 0.01$). F, SUM159 and BT549 cells were treated with 100 nmol/L MLN128 for 0.5, 3, 24, 48, and 72 hours, followed by immunoblot analysis for NICD, actin, and phospho-S6. G, SUM159 cells were transfected with control, Rictor, Raptor, or both Rictor and Raptor siRNAs for 72 hours. Immunoblot analysis was performed using the indicated antibodies. FACS analysis for ALDH positivity was also performed at the same time point as shown on the right (*, $P = 0.008$). Error bars, mean ± SEM.

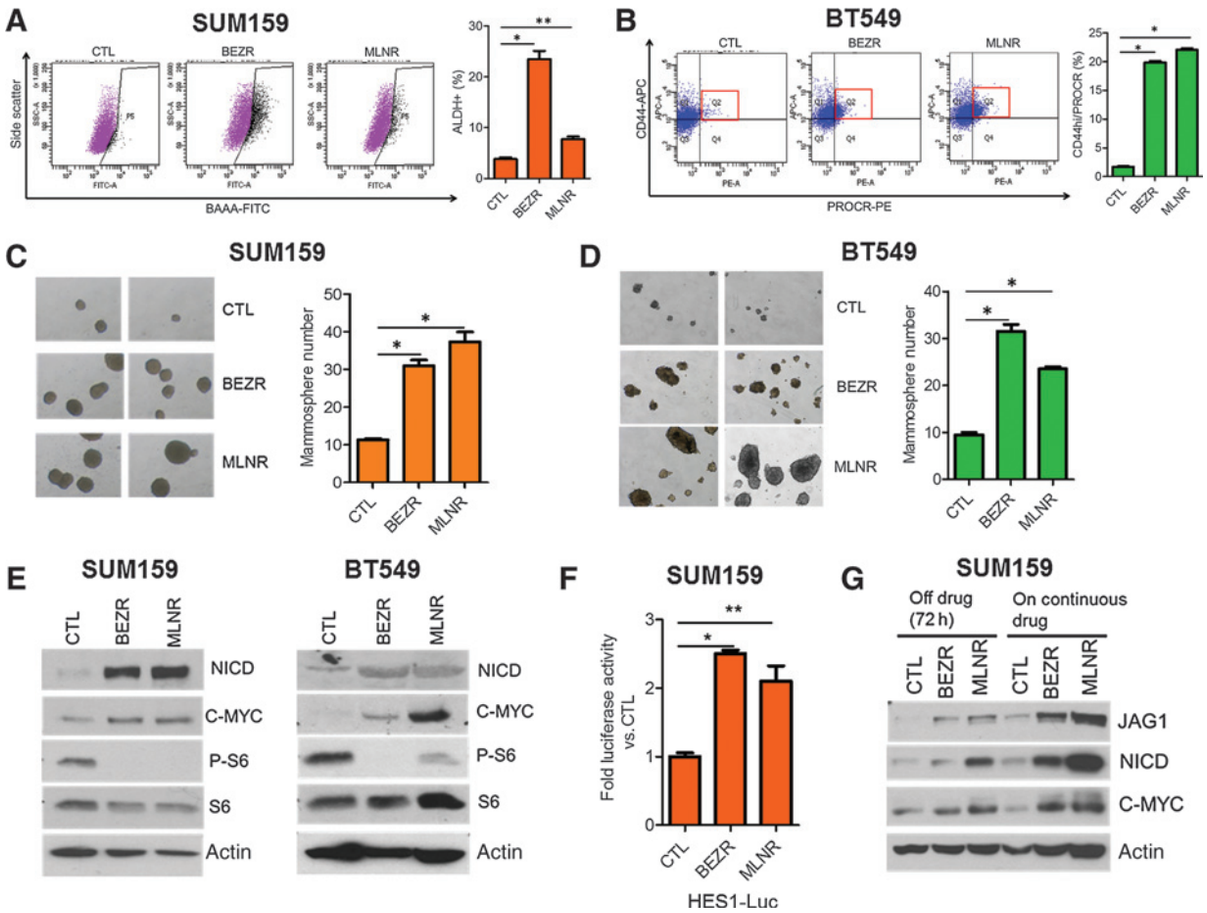


**Figure 3.**

Persistent TORC1/2 inhibition drives Notch1 signaling and a CSC-like phenotype. A, SUM159 and B, BT549 cells were treated with progressively higher concentrations (50–300 nmol/L) of BEZ235 (BEZR) and MLN128 (MLNR) over a period of 8 weeks. FACS analysis for the CSC markers was quantified (SUM159: *, $P = 0.0002$; **, $P = 0.002$; BT549: *, $P < 0.03$). C, SUM159 and D, BT549 cells were treated as described in A and B and seeded as mammospheres; mammosphere number was determined after 7 days using GelCount (SUM159: *, $P < 0.01$; BT549: *, $P < 0.02$). Two representative images of mammospheres from each treatment are shown (magnification, ×40). E, immunoblot analysis of SUM159 and BT549 BEZR and MLNR cells was performed using the indicated antibodies. F, SUM159, BEZR, and MLNR cells were transfected with the HES1-*Firefly* Luciferase and CMV-*Renilla* constructs. The Dual Luciferase Assay was performed after 48 hours as described in Materials and Methods (*, $P < 0.0001$; **, $P = 0.03$). G, SUM159 CTL, BEZR, and MLNR cells were cultured in the continuous presence of vehicle or their respective inhibitor or taken off drug selection for 72 hours, followed by immunoblot analysis for NICD, C-MYC, and JAG1. Error bars, mean ± SEM.

BEZ235 and MLN128, respectively, retained the Cell Tracker dye compared with <5% of untreated cells (Supplementary Fig. S1B). These results suggest that pharmacologic inhibition of TORC1/2 in TNBC cells results in the survival of a cell population with CSC-like features.

### Inhibition of TORC1/2 increases Notch1 signaling

In order to identify genes associated with CSCs surviving TORC1/2 inhibition, we used a Cancer Stem Cell–specific PCR array. SUM159 cells were treated with MLN128 for 48 hours and assessed for changes in CSC gene expression. Notch1, Jagged1 (JAG1), POUF51 (OCT4), MUC1, and MYC expression was increased >2-fold upon MLN128 treatment, with Notch1 being the top hit with a near 4-fold induction (Fig. 2A). Supporting the array data, treatment of six TNBC cell lines with each BEZ235 and MLN128 for 72 hours induced Notch1 mRNA levels anywhere from 2- to >20-fold as measured by qPCR (Fig. 2B). Using a separate Stem Cell–specific PCR array to confirm these findings, both Notch1 and JAG1 were induced >1.5-fold upon BEZ235 treatment of SUM159 cells (Supplementary Fig. S2A). In the Stem Cell PCR array, a 10-fold increase in FGF1 mRNA was observed, which was confirmed in SUM159 and BT549 cells treated with each BEZ235 and MLN128 for 3 to 48 hours (Supplementary Fig. S2B and S2C). A similar induction of FGF1 mRNA was seen in MLN128-treated CAL51, CAL120, and MDA468 but not in MDA231 cells (Supplementary Fig. S2D and S2E). Concurrent with the induction of Notch1 mRNA, BEZ235 and MLN128 treatment increased expression of the active Notch1 intracellular domain (NICD). Drug-induced NICD expression was ablated by the γ-secretase inhibitor GSI-IX, which prevents the cleavage of full-length Notch1 (Fig. 2C). In addition, protein expression of the Notch ligand JAG1 was increased in BEZ235- and MLN128-

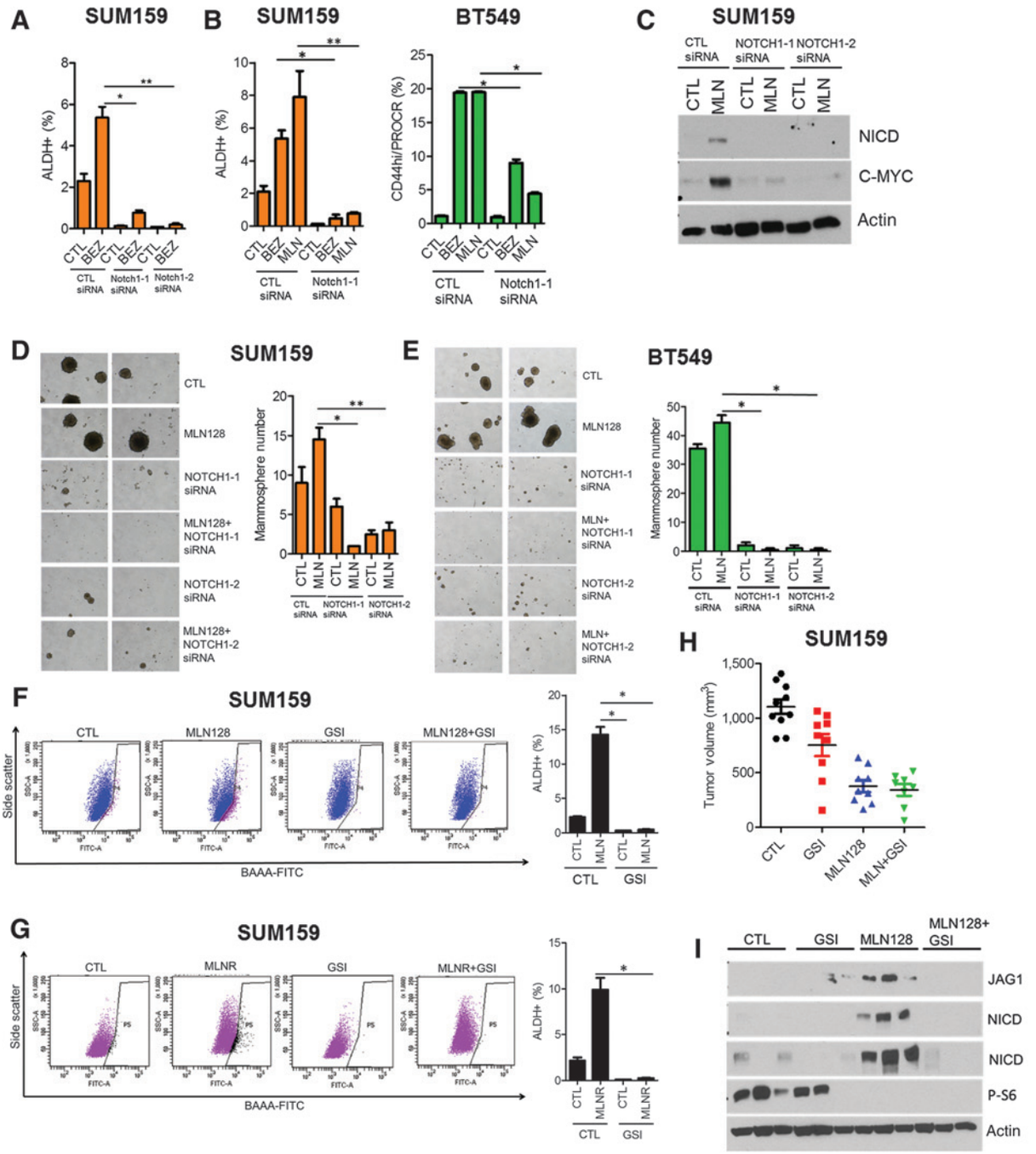


| Cells seeded | Control | MLN128 | GSI | MLN128 +GSI |
|---|---|---|---|---|
| 5000 | 5/10 | 9/10 | 3/10 | 5/10 |
| 500 | 3/10 | 5/10 | 0/10 | 1/10 |
| 50 | 0/10 | 2/10 | 0/10 | 1/10 |
| CSC frequency (1 in..) | 1/5025 | 1/1201 | 1/15869 | 1/5852 |

| Group 1 | Group 2 | *P* |
|---|---|---|
| Control | MLN128 | 0.00238 |
| Control | GSI | 0.0735 |
| Control | MLN128+GSI | 0.773 |
| MLN128 | GSI | 0.000004 |
| MLN128 | MLN128+GSI | 0.00102 |
| GSI | MLN128+GSI | 0.133 |

treated TNBC cells (Fig. 2D). Drug-induced Notch1 activation was associated with increased expression of the classical Notch target genes *HES1* and *HEY2* (Fig. 2E). Furthermore, BT549, MDA468, and SUM159 cells transfected with a NICD-responsive transcriptional reporter displayed increased reporter activity upon 17- to 48-hour treatment with BEZ235 and MLN128 (Supplementary Fig. S2F and S2G). MLN128-induced treatment was time dependent, being detected at 24 hours and increasing up to 72 hours (Fig. 2F). To genetically replicate TORC1/2 inhibition, we downmodulated Rictor (TORC2) and Raptor (TORC1) expression with siRNA. Dual knockdown of Rictor and Raptor augmented NICD expression and the $ALDH^+$ population in SUM159 cells; these were not observed with Rictor or Raptor siRNA alone (Fig. 2G). These data suggest that TORC1/2 inhibition induces expression of CSC genes Notch1 and Jag1, the stem cell gene FGF1, and activates Notch signaling.

Next, we investigated whether chronic inhibition of TORC1/2 also induces a CSC phenotype and Notch1 activity. SUM159 and BT549 cells were maintained in gradually increasing concentrations (50–300 nmol/L) of BEZ235 and MLN128 for a period of 2 months. BEZ235- and MLN128-resistant (BEZR and MLNR) SUM159 and BT549 cells displayed increased CSC markers (Fig. 3A and B) and mammosphere-forming capacity compared with untreated control cells (Fig. 3C and D). This was associated with increased expression of NICD, JAG1, and the Notch1 transcriptional target c-MYC (Fig. 3E), and HES1 luciferase reporter activity (Fig. 3F) in BEZR and MLNR cells compared with their respective untreated controls. BEZR and MLNR cells withdrawn from their respective inhibitor for 72 hours continued to exhibit higher levels of NICD, JAG1, and c-MYC (Fig. 3G). These results suggest that, similar to acute treatment, chronic inhibition of TORC1/2 in TNBC cells sustains a surviving population of CSCs with activated Notch.

Finally, we examined whether a similar enrichment of Notch-activated CSCs occurred with other anticancer therapies. Other studies with TNBC cells have suggested that cells resistant to chemotherapy exhibit cancer stem-like features (19, 23). RNA extracted from 17 matched primary breast tumor biopsies before and after neoadjuvant chemotherapy was subjected to Nanostring analysis. Notch1 and JAG1 mRNA expression was significantly higher in post-chemotherapy, drug-resistant tumors (Supplementary Fig. S3A). Paclitaxel is one of the most commonly used chemotherapeutics in TNBC. Consistent with the primary breast tumor data, paclitaxel treatment of SUM159 cells increased NICD expression (Supplementary Fig. S3B). The combination of paclitaxel with each BEZ235 and MLN128 inhibited SUM159 growth more potently than each drug alone (Supplementary Fig. S3C). However, the cells surviving the combination displayed increased ALDH positivity and mammosphere formation (Supplementary Fig. S3D and S3E). The combination of paclitaxel and MLN128 induced an increase in NICD expression in SUM159 cells, which was abrogated with a γ-secretase inhibitor (Supplementary Fig. S3F). These data also suggest that TORC1/2 inhibitors and anticancer chemotherapeutics result in a resistant Notch1-driven CSC population.

### Blockade of Notch1 decreases the CSC population induced by TORC1/2 inhibition

To establish a causal association between Notch1 activity and the CSCs induced by TORC1/2 inhibition, we blocked Notch1 both genetically and pharmacologically. Knockdown of Notch1 using two siRNAs decreased BEZ235 and MLN128-induced CSCs in both SUM159 and BT549 lines as determined by FACS (Fig. 4A and B). Notch1 downmodulation also decreased the $ALDH^+$ population in SUM159 MLNR cells (Supplementary Fig. S4A) and abrogated MLN128-induced NICD expression in SUM159 cells (Fig. 4C). In both SUM159 and BT549 cells, Notch1 knockdown with two siRNAs completely blunted MLN128-induced mammosphere formation (Fig. 4D and E). Furthermore, siRNA-mediated downmodulation of the Notch1 ligand JAG1 decreased MLN128-induced NICD expression and mammosphere formation (Supplementary Fig. S4B). These results suggest that genetic targeting of Notch1 and its ligand JAG1 abrogate the surviving CSC population following TORC1/2 inhibition.

To pharmacologically block Notch, we employed the γ-secretase inhibitor GSI-IX (GSI). Using FACS, treatment with GSI-IX markedly decreased SUM159 and BT549 CSCs induced by acute MLN128 treatment (Fig. 4F and Supplementary Fig. S4C) as well as SUM159 MLNR CSCs induced by chronic MLN128 treatment (Fig. 4G). To examine the effect of Notch inhibition *in vivo*, nude mice were injected with SUM159 cells in the #4 mammary gland. Once tumors reached $\geq$75 $mm^3$, mice were randomized to treatment with (i) vehicle, (ii) MLN128, (iii) GSI, or (iv) MLN128 + GSI. After 28 days, MLN128 treatment reduced tumor growth by 60% compared with vehicle-treated tumors; the combination of MLN128 and GSI did not enhance the anti-tumor effect of MLN128 alone (Fig. 4H). Immunoblot analysis of MLN128-treated tumor lysates displayed increased NICD and JAG1 expression, which were undetectable in tumors treated with MLN128 and GSI (Fig. 4I). Next, we performed a limiting dilution assay to assess the tumorigenic capacity of cancer cells in the treated xenografts. Tumors from all four treatment groups were harvested after 28 days; single cells were prepared and injected in limiting dilutions (50–5,000) into tumor-free mice. SUM159 cells from

**Figure 4.**

Notch1 downmodulation decreases the induction of CSCs upon inhibition of TORC1/2. A, SUM159 cells were transfected with two different Notch1 siRNAs ± 250 nmol/L BEZ235 for 72 hours. FACS analysis for $ALDH^+$ cells was performed (*, $P < 0.03$; **, $P < 0.001$). B, SUM159 and BT549 cells were transfected with Notch1 siRNA ± 250 nmol/L BEZ235 or 100 nmol/L MLN128. After 72 hours, FACS analysis for $ALDH^+$ or $CD44hi/PROCR^+$ expression was performed (*, $P < 0.03$; **, $P < 0.001$). C, SUM159 cells were transfected with two Notch1 siRNAs ± 100 nmol/L MLN128. After 72 hours, immunoblot analysis for NICD, C-MYC, and actin expression was performed. D and E, SUM159 (D) and BT549 (E) cells were transfected with Notch1 siRNAs ± 100 nmol/L MLN128 for 48 hours. Cells were trypsinized and seeded as mammospheres. After 7 days, mammosphere number was determined (*, $P < 0.03$; **, $P < 0.001$). F, SUM159 cells were treated with 100 nmol/L MLN128 and/or 5 μmol/L GSI-IX for 72 hours, followed by FACS analysis for ALDH positivity (*, $P < 0.01$). G, SUM159 CTL and MLNR cells were treated with 5 μmol/L GSI-IX for 72 hours, followed by FACS analysis for ALDH positivity (*, $P < 0.01$). H, SUM159 xenografts were divided into four treatment groups ($n = 10$): vehicle, MLN128 (1 mg/kg ×3/week, orally), GSI-IX (10 mg/kg, 3 days on, 4 days off, i.p.), MLN128 + GSI-IX. Tumor volumes of individual xenografts at day 28 are represented. I, lysates from xenografts in each treatment group were analyzed for NICD, JAG1, phospho-S6, and actin. J, *in vivo* limiting dilution experiment to determine tumor incidence from SUM159 xenografts treated with vehicle, MLN128, GSI-IX, and MLN128 + GSI-IX. *P* values for pair-wise statistical analysis of treatment groups were determined by ELDA and displayed. Fold change in tumor-initiating frequency is represented by the bar graph (right). Error bars, mean ± SEM.

MLN128-treated xenografts displayed a >4-fold greater tumorigenic potential *in vivo* compared with cells from vehicle-treated xenografts ($P = 0.002$; Fig. 4J). This increase in CSC frequency was markedly reduced in cells from tumors that had been treated with MLN128 + GSI ($P = 0.001$; Fig. 4J). A similar experiment was performed with MDA468 cells. MLN128 treatment decreased growth of MDA468 xenografts (Supplementary Fig. S4D) but enriched for a tumorigenic CSC population in residual drug-resistant tumors. This population was markedly reduced in MLN128+GSI-treated tumors ($P = 0.00001$; Supplementary Fig. S4E). These results suggest TORC1/2 inhibition enriches a Notch1-dependent tumor-initiating population

**Notch1 activity induced upon TORC1/2 is dependent on mitochondrial metabolism**

To explore mechanisms by which TORC1/2 inhibitors enrich a Notch1-dependent CSC population, we examined metabolic alterations associated with the induction of Notch1 activity and CSCs. A link with cellular metabolisms is suggested by a recent study in pancreatic cancer showed that cells surviving MEK inhibition or KRAS depletion displayed increased mitochondrial metabolism and tumorigenic potential (24). SUM159 and BT549 cells treated with MLN128 expressed increased levels of the mitochondrial stain Mitotracker Red, which is used as readout of mitochondrial membrane potential (Fig. 5A). To determine whether the increased Mitotracker Red staining was due to increased mitochondrial biogenesis, we performed TEM of MLN128-treated SUM159 cells. In MLN128-treated cells, we observed increased mitochondrial number and increased microlipophagy (lipid droplet fusions; Supplementary Fig. S5A). Similar results were obtained with BEZ235-treated cells (data not shown). In addition to increased mitochondrial mass, BEZ235 and MLN128 treatment increased the expression of the mitochondrial DNA transcription factor, Transcription factor A mitochondrial (TFAM; Fig. 5B). To extend on this induction of TFAM, we performed a Mitochondrial Metabolism PCR Array using SUM159 and BT549 cells. Polycistronic mitochondrial transcripts from both the H1 and H2 promoter sites of the Heavy (H) strand of the mitochondrial genome were increased >2-fold after 3 and 48 hours of MLN128 treatment compared with vehicle-treated cells (Fig. 5C; Supplementary Fig. S5B and S5C). TFAM has been shown to be critical for the production of transcripts from the mitochondrial H strand promoter (25). ATP synthase complex subunits are critical for utilizing the mitochondrial membrane potential alteration during oxidative phosphorylation to generate ATP (26). Expression of the ATP synthase complex subunits (ATP5G2 and ATP5J2) were also upregulated >2-fold in both MLN128-treated SUM159 and BT549 cells (Fig. 5C; Supplementary Fig. S5B and S5C).

To determine if the induction of TFAM and oxidative phosphorylation played a role on CSC induction, we combined MLN128 with two different TFAM siRNAs or with Oligomycin A (ATP synthase inhibitor). TFAM siRNA and Oligomycin A decreased the $ALDH^+$ population and NICD induced by MLN128 (Fig. 5D and E). TFAM siRNA also enhanced the inhibition of SUM159 cell viability induced by each BEZ235 and MLN128 compared with each drug alone (Supplementary Fig. S5D). To further support that the inhibition of mitochondrial activity and of oxidative phosphorylation blocked the induction of CSCs upon treatment with the TORC1/2 inhibitor by trumping Notch activation, we rescued Notch1 activity with a GFP-expressing human NICD vector (Fig. 5F). In SUM159 cells cotreated with MLN128 and Oligomycin A, transfection of GFP-hNICD restored the induction of CD44hi expression and mammosphere formation (Fig. 5G). Next, we treated BT549 cells with MLN128 and TFAM siRNA in the presence or absence of a control vector or hNICD. TFAM knockdown decreased MLN128-induced CD44hi cells, but transfection of hNICD restored the CD44hi fraction (Supplementary Fig. S5E). These results suggest that TORC1/2 inhibition augments mitochondrial biogenesis, transcription, and metabolism, which are important for CSC survival and Notch1 activity.

**MLN128-mediated Notch1 activity is dependent on FGFR signaling**

With the link between mitochondrial metabolism and Notch activity, we next inquired whether induction of the stem cell gene FGF1 (Supplementary Fig. S2) participated in the interaction of these pathways. In a panel of five TNBC cell lines, acute treatment with MLN128 increased levels of full-length and/or the cleaved form of FGFR1 (Fig. 6A). FGFR2, 3, and 4 were undetectable by immunoblot analysis, with the exception of CAL51 (FGFR2, FGFR3). However, MLN128 did not alter FGFR2 and FGFR3 expression in CAL51 cells (data not shown). We next determined whether FGFR1 expression was necessary for MLN128-induced NICD expression and mitochondrial activity. FGFR1 siRNA decreased NICD and TFAM induction in both MLN128-treated SUM159 and BT549 cells (Fig. 6B). Further, MLN128-treated SUM159 cells displayed increased Mitotracker Red expression, which was significantly decreased by FGFR1 siRNA (Fig. 6C). Menadione, which decreases mitochondrial potential, was used as a positive control for Mitotracker expression. FGFR1 siRNA also reduced the MLN128-induced CD44hi BT549 cell population; this effect of MLN128 was restored by exogenous expression of hNICD (Fig. 6D). To assess whether FGFR activation was also involved, we used the FGFR tyrosine kinase inhibitor (TKI) lucitanib (27, 28) and siRNA targeted against the FGFR adaptor protein FRS2. FRS2 knockdown by RNAi was confirmed by qPCR (Fig. 6F). In both SUM159 and BT549 cells, MLN128-induced NICD expression was abrogated by both FRS2 siRNA and by lucitanib treatment (Fig. 6E). Similar results were observed with MDA468 cells treated with MLN128 and lucitanib (Supplementary Fig. S6A). Additionally, FRS2 siRNA decreased MLN128-induced TFAM expression (Supplementary Fig. S6B). Lucitanib treatment also abrogated MLN128-induced $ALDH^+$ SUM159 cells and CD44hi/CD24lo MDA468 cells (Fig. 6G). These observations suggest that FGFR activity plays a causal role in mediating mitochondrial and Notch1 activity as well as the induction of CSCs upon TORC1/2 inhibition (Fig. 6H).

## Discussion

In this study, we observed that TORC1/2 inhibition resulted in decreased survival/growth of TNBC cancer cells both *in vitro* and *in vivo* but spared a population with CSC-like properties and enhanced Notch1 activity. Both genetic and pharmacologic inhibition of Notch1 blunted the CSCs induced upon inhibition of TORC1/2. This CSC-like population that survives TORC1/2 inhibition is driven by a FGFR1–TFAM–Notch1 signaling axis. Activation of Notch1 was not limited to TNBC as inhibition of TORC1/2 in head and neck cancer and ovarian cancer cells also resulted in activation of Notch1 (data not shown). From a clinical

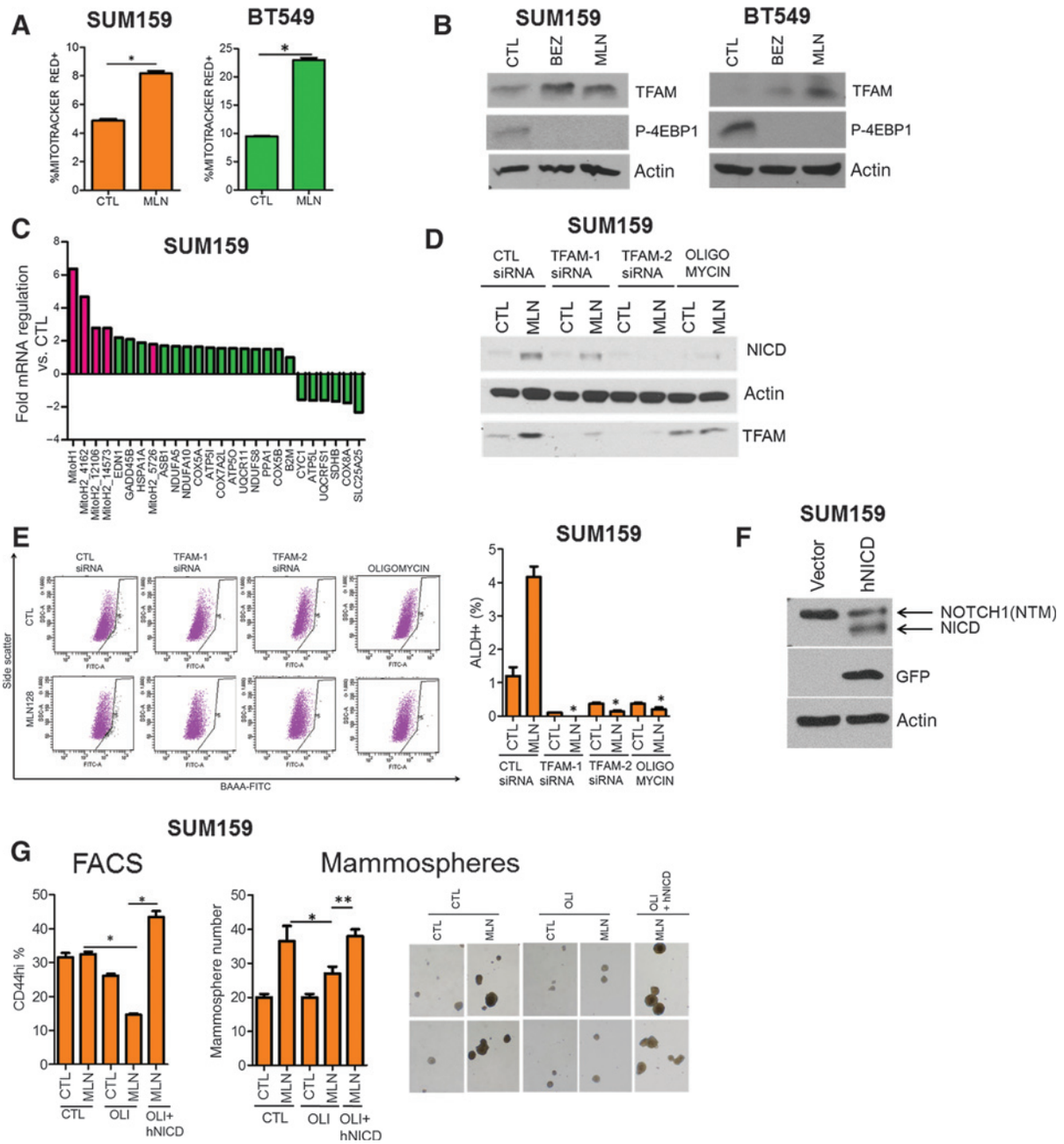


**Figure 5.**

Induction of NICD and CSCs following TORC1/2 inhibition is dependent on mitochondrial metabolism. A, SUM159 and BT549 cells were treated with control or 100 nmol/L MLN128 for 48 hours. Cells were stained with a marker for mitochondrial membrane potential Mitotracker Red-CMXRos and analyzed by flow cytometry. The percentage of Mitotracker Red-positive cells was determined (*, $P < 0.0008$). B, SUM159 and BT549 cells were treated with vehicle, 250 nmol/L BEZ235, or 100 nmol/L MLN128 for 72 hours. Immunoblot analysis for TFAM, phospho-4EBP1, and actin was performed. C, SUM159 cells were treated with vehicle or 100 nmol/L MLN128 for 48 hours. RNA was extracted, transcribed to cDNA, and applied to a Mitochondrial Metabolism PCR Array. Genes displaying fold changes greater or lower than 1.5 compared with vehicle-treated cells were illustrated. Red highlighted bars indicate mitochondrial polycistronic transcripts. D, immunoblot analysis of SUM159 cells transfected with control or TFAM siRNA, treated with 500 nmol/L oligomycin ± 100 nmol/L MLN128 for 72 hours. E, SUM159 cells were transfected with control or 2 TFAM siRNAs or treated with 500 nmol/L oligomycin A (OLI) ± 100 nmol/L MLN128 for 72 hours. FACS analysis for $ALDH^+$ cells was performed (*, $P < 0.006$). F, SUM159 cells transfected with empty vector and hNICD vector was analyzed by immunoblotting (NTM–Notch transmembrane). G, SUM159 cells were transfected with control vector or human NICD (hNICD) followed by treatment with vehicle or MLN128 ± 500 nmol/L oligomycin (OLI). After 72 hours, the CD44hi cells were identified by FACS (*, $P < 0.003$) or seeded as mammospheres and cultured for 10 days. Mammosphere number was determined using Gelcount (*, $P = 0.01$; **, $P = 0.001$). Two representative images of mammospheres from each treatment group are illustrated (magnification, ×40). Error bars, mean ± SEM.

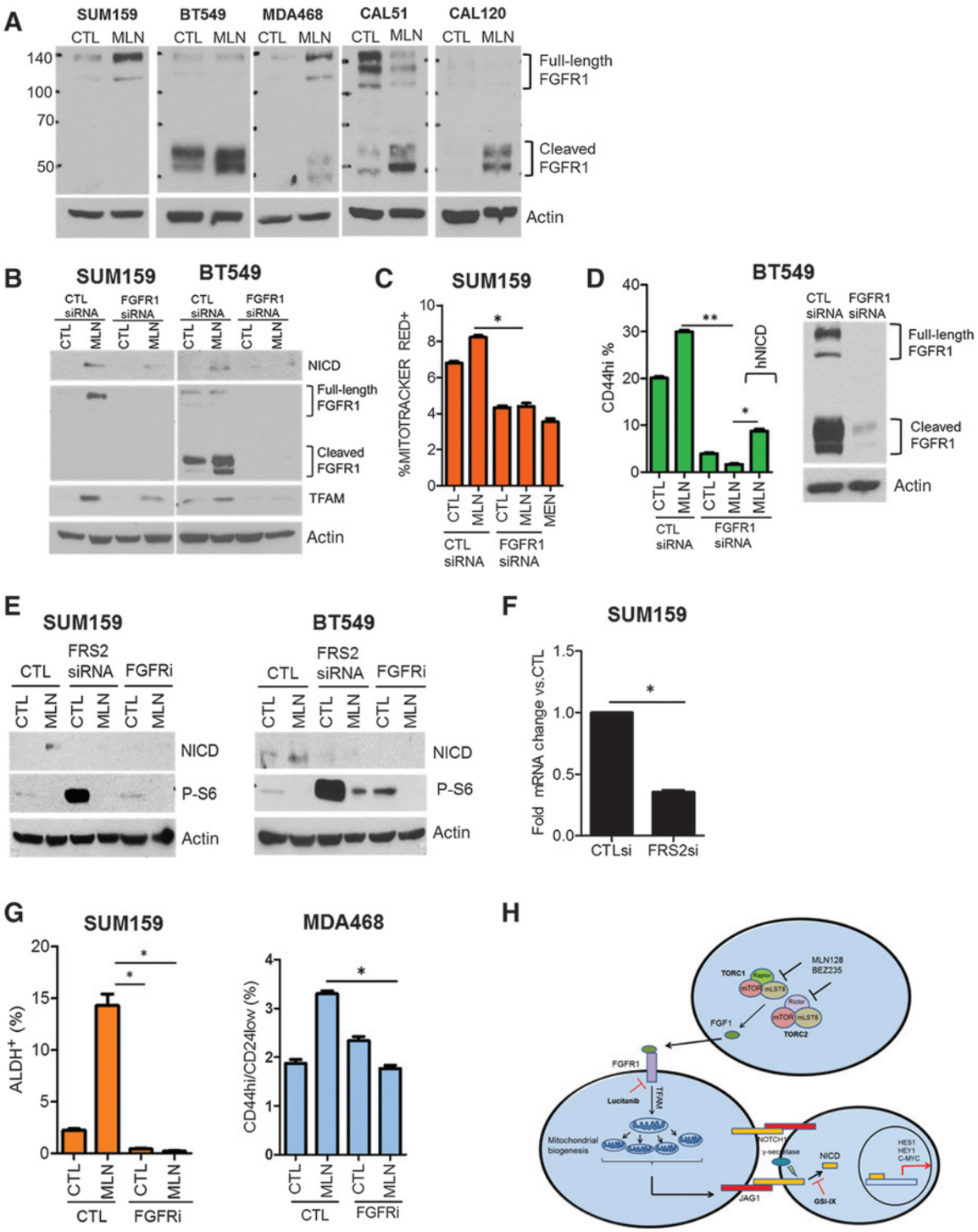


**Figure 6.**
Induction of Notch1 and CSCs upon inhibition of TORC1/2 is FGFR dependent. A, SUM159, BT549, MDA468, CAL51, and CAL120 cells were treated with 100 nmol/L MLN128 for 72 hours. Immunoblot analysis for FGFR1 and actin was performed. B, SUM159 and BT549 cells were transfected with control or FGFR1siRNA ± 100 nmol/L MLN128 for 72 hours. Immunoblot analysis for NICD, FGFR1, TFAM, and actin was performed. C, SUM159 cells were transfected with control or FGFR1siRNA ± 100 nmol/L MLN128 for 48 hours. FACS analysis for Mitotracker Red was performed. Cells were treated with 5 μmol/L menadione as a positive control (*, $P = 0.003$). D, BT549 cells were transfected with control vector or GFP-hNICD followed by transfection with CTL or FGFR1 siRNA ± MLN128. After 72 hours, FACS analysis for CD44hi cells was performed (*, $P = 0.002$; **, $P < 0.001$). E, SUM159 and BT549 cells were transiently transfected with CTL and FRS2 siRNA or treated with 2 μmol/L lucitanib for 72 hours. Immunoblot analysis for NICD, phospho-S6, and actin expression was performed. F, SUM159 cells were transfected with CTL and FRS2 siRNA for 48 hours followed by qPCR analysis for FRS2 expression (*, $P = 0.0003$). G, SUM159 and MDA468 cells were treated with 100 nmol/L MLN128 and/or 2 μmol/L lucitanib for 72 hours. FACS analysis for CSC markers was performed (*, $P < 0.02$). Error bars, mean ± SEM. H, proposed mechanistic model of NICD and CSC induction following TORC1/2 inhibition in TNBC.

perspective, these findings underscore a limitation of TORC1/2 inhibitors in cancer because of their ability to induce a signaling nexus that drives the survival of cells with stem-like and tumor-initiating properties. TORC1 inhibition with rapamycin increases the lifespan of mice by increasing the self-renewal and hematopoiesis of hematopoietic stem cells (29). Chronic rapamycin treatment, which by disrupting the raptor/mTOR complex also inhibits TORC2 (30), has been shown to increase animal lifespan by enhancing stem cell survival (31). These observations combined with our findings suggest that TORC1/2 inhibition results in sustenance of a stem cell-like population. This is also important because the pathways used to prevent aging can be exploited as molecular targets, which, once inhibited, would also limit expansion of a CSC population.

In this study, we provide evidence that TORC1/2 inhibition promotes the survival of cells with increased mitochondrial mass and metabolism, which are required for the maintenance of CSCs. A report in pancreatic cancer illustrated that KRAS loss results in the survival of cells with increased mitochondrial metabolism (24). Additionally, the KRAS-deficient surviving cells were tumorigenic and sensitive to inhibition of oxidative phosphorylation. Another study showed that conditional loss of TFAM in keratinocytes decreased two Notch1 transcriptional targets Hes1 and Hey2 (32). Therefore, a tumorigenic population of cells can utilize a mitochondrial-dependent Notch1 axis to survive anticancer therapies. However, the exact mechanism by which oxidative phosphorylation or mitochondrial biogenesis regulates Notch1 activation warrants further investigation.

FGF1 expression was potently induced in several TNBC cell lines upon inhibition of TORC1/2. This is consistent with a recent report by Wilson and colleagues that showed that FGFR ligands can blunt the efficacy of several kinase inhibitors across multiple oncogene-dependent tumor cell lines (33). Another report showed that treatment of $HER2^{+}$ breast cancer cells with the HER2 inhibitor lapatinib increased the expression of FGFR1 as a mechanism of lapatinib resistance (30). In the study herein, both genetic and pharmacologic inhibition of FGFR decreased MLN128-induced TFAM expression and mitochondrial metabolism (Fig. 6). The link between FGFR1 and mitochondrial activity is consistent with a report using FGFR1-amplified lung cancer and leukemia cell lines. In this study, FGFR1 was shown to localize in mitochondria and phosphorylate pyruvate dehydrogenase kinase 1 (PDHK1). The inactivating phosphorylation of PDHK1 results in activation of the pyruvate dehydrogenase complex, which, in turn, drives the conversion of pyruvate to acetyl-CoA and favor oxidative phosphorylation (34). In multiple TNBC cell lines we observed increased expression of the cleaved form of FGFR1 upon MLN128 treatment. This cleaved form of FGFR1 has been shown to localize in the nucleus and mitochondria, where it mediates oxidative phosphorylation and induces cellular invasion (34, 35). Thus, activation of Notch1 via increased mitochondrial metabolism may be a key event in resistance to anticancer therapies. The mechanism by which FGFR1 regulates TFAM expression remains to be investigated.

In summary, we have identified a mechanism by which TORC1/2 inhibitors sustain a Notch1-dependent tumorigenic population with CSC traits. We propose that this mechanism explains at least in part the limited clinical activity of these drugs as single agents. As a result, therapeutic targeting of Notch1 may be a promising direction to limit this tumor-initiating population and potentially enhance the antitumor effect of TORC1/2 inhibitors in TNBC. Additionally, we have shown that Notch1 is activated via a FGFR1–TFAM-dependent mechanism introducing additional molecular targets (Fig. 6H) that can be exploited in clinical trials in tumors with alterations in the PI3K/mTOR pathway.

## Disclosure of Potential Conflicts of Interest

No potential conflicts of interest were disclosed.

## Authors' Contributions

**Conception and design:** N.E. Bhola, C.L. Arteaga
**Development of methodology:** N.E. Bhola
**Acquisition of data (provided animals, acquired and managed patients, provided facilities, etc.):** N.E. Bhola, V.M. Jansen, J.P. Koch, H. Li, L. Formisano, J.A. Williams, J.R. Grandis, C.L. Arteaga
**Analysis and interpretation of data (e.g., statistical analysis, biostatistics, computational analysis):** N.E. Bhola, L. Formisano, J.R. Grandis, C.L. Arteaga
**Writing, review, and/or revision of the manuscript:** N.E. Bhola, C.L. Arteaga
**Administrative, technical, or material support (i.e., reporting or organizing data, constructing databases):** N.E. Bhola, V.M. Jansen, J.P. Koch, C.L. Arteaga
**Study supervision:** N.E. Bhola, C.L. Arteaga

## Acknowledgments

Electron microscopy data acquisition and analysis were performed through the Vanderbilt Cell Imaging Shared Resource. Flow Cytometry experiments were performed in the VMC Flow Cytometry Shared Resource. The authors thank Dr. Christian Young and Dr. Monica Red-Brewer for helpful discussions and review of this article.

## Grant Support

This work was supported by Breast SPORE P50 CA98131, Vanderbilt-Ingram Cancer Center Support Grant P30 CA68485, Susan G. Komen Grant SAC100013 (C.L. Arteaga), Susan G. Komen Post-doctoral Fellowship (PDF12227859), NIH R01DE023685 (J.R. Grandis), and P50CA097190 (J.R. Grandis).

The costs of publication of this article were defrayed in part by the payment of page charges. This article must therefore be hereby marked *advertisement* in accordance with 18 U.S.C. Section 1734 solely to indicate this fact.

Received June 16, 2015; revised August 25, 2015; accepted October 1, 2015; published OnlineFirst December 16, 2015.

## References

1. Bertucci F, Finetti P, Cervera N, Esterni B, Hermitte F, Viens P, et al. How basal are triple-negative breast cancers? Int J Cancer 2008;123:236–40.
2. Liedtke C, Mazouni C, Hess K, Andre F, Tordai A, Mejia J, et al. Response to neoadjuvant therapy and long-term survival in patients with triple-negative breast cancer. J Clin Oncol 2008;26:1275–81.
3. Banerji S, Cibulskis K, Rangel-Escareno C, Brown KK, Carter SL, Frederick AM, et al. Sequence analysis of mutations and translocations across breast cancer subtypes. Nature 2012;486:405–9.
4. Lehmann BD, Bauer JA, Chen X, Sanders ME, Chakravarthy AB, Shyr Y, et al. Identification of human triple-negative breast cancer subtypes and preclinical models for selection of targeted therapies. J Clin Invest 2011;121:2750–67.
5. Shah S, Morin R, Khattra J, Prentice L, Pugh T, Burleigh A, et al. Mutational evolution in a lobular breast tumour profiled at single nucleotide resolution. Nature 2009;461:809–13.
6. TCGA. Comprehensive molecular portraits of human breast tumours. Nature 2012;490:61–70.

7. Győrffy B, Lanczky A, Eklund A, Denkert C, Budczies J, Li Q, et al. An online survival analysis tool to rapidly assess the effect of 22,277 genes on breast cancer prognosis using microarray data of 1,809 patients. Breast Cancer Res Treat 2010;123:725–31.
8. Shimobayashi M, Hall MN. Making new contacts: the mTOR network in metabolism and signalling crosstalk. Nat Rev Mol Cell Biol 2014;15: 155–62.
9. Thorpe LM, Yuzugullu H, Zhao JJ. PI3K in cancer: divergent roles of isoforms, modes of activation and therapeutic targeting. Nat Rev Cancer 2015;15:7–24.
10. Zhang H, Cohen A, Krishnakumar S, Wapnir I, Veeriah S, Deng G, et al. Patient-derived xenografts of triple-negative breast cancer reproduce molecular features of patient tumors and respond to mTOR inhibition. Breast Cancer Res 2014;16:R36.
11. Britschgi A, Andraos R, Brinkhaus H, Klebba I, Romanet V, Müller U, et al. JAK2/STAT5 inhibition circumvents resistance to PI3K/mTOR blockade: a rationale for cotargeting these pathways in metastatic breast cancer. Cancer Cell 2012;22:796–811.
12. Ilic N, Utermark T, Widlund HR, Roberts TM. PI3K-targeted therapy can be evaded by gene amplification along the MYC-eukaryotic translation initiation factor 4E (eIF4E) axis. Proc Natl Acad Sci 2011;108:E699–E708.
13. Roper J, Richardson MP, Wang WV, Richard LG, Chen W, Coffee EM, et al. The dual PI3K/mTOR inhibitor NVP-BEZ235 induces tumor regression in a genetically engineered mouse model of *PIK3CA* wild-type colorectal cancer. PLoS One 2011;6:e25132.
14. Cho DC, Cohen MB, Panka DJ, Collins M, Ghebremichael M, Atkins MB, et al. The efficacy of the novel dual PI3-kinase/mTOR inhibitor NVP-BEZ235 compared to rapamycin in renal cell carcinoma. Clin Cancer Res 2010;16:3628–38.
15. Al-Hajj M, Wicha MS, Benito-Hernandez A, Morrison SJ, Clarke MF. Prospective identification of tumorigenic breast cancer cells. Proc Natl Acad Sci U S A 2003;100:3983–8.
16. McDermott SP, Wicha MS. Targeting breast cancer stem cells. Mol Oncol 2010;4:404–19.
17. Yu X, Alder JK, Chun JH, Friedman AD, Heimfeld S, Cheng L, et al. HES1 inhibits cycling of hematopoietic progenitor cells via DNA binding. Stem Cells 2006;24:876–88.
18. Saxena MT, Schroeter EH, Mumm JS, Kopan R. Murine notch homologs (N1–4) undergo presenilin-dependent proteolysis. J Biol Chem 2001;276: 40268–73.
19. Bhola NE, Balko JM, Dugger TC, Kuba G, Sanchez V, Sanders M, et al. TGF-$\beta$ inhibition enhances chemotherapy action against triple-negative breast cancer. J Clin Invest 2013;123:1348–58.
20. Hu Y, Smyth GK. ELDA: extreme limiting dilution analysis for comparing depleted and enriched populations in stem cell and other assays. J Immunol Methods 2009;347:70–8.
21. Roesch A, Fukunaga-Kalabis M, Schmidt EC, Zabierowski SE, Brafford PA, Vultur A, et al. A temporarily distinct subpopulation of slow-cycling melanoma cells is required for continuous tumor growth. Cell 2010;141:583–94.
22. Xin H-W, Hari DM, Mullinax JE, Ambe CM, Koizumi T, Ray S, et al. Tumor-initiating label-retaining cancer cells in human gastrointestinal cancers undergo asymmetric cell division. Stem Cells 2012;30:591–8.
23. Gupta PB, Onder TT, Jiang G, Tao K, Kuperwasser C, Weinberg RA, et al. Identification of selective inhibitors of cancer stem cells by high-throughput screening. Cell 2009;138:645–59.
24. Viale A, Pettazzoni P, Lyssiotis CA, Ying H, Sanchez N, Marchesini M, et al. Oncogene ablation-resistant pancreatic cancer cells depend on mitochondrial function. Nature 2014;514:628–32.
25. Ngo HB, Lovely GA, Phillips R, Chan DC. Distinct structural features of TFAM drive mitochondrial DNA packaging versus transcriptional activation. Nat Commun 2014;5: 3077.
26. Yoshida M, Muneyuki E, Hisabori T. ATP synthase—a marvellous rotary engine of the cell. Nat Rev Mol Cell Biol 2001;2:669–77.
27. Bello E, Colella G, Scarlato V, Oliva P, Berndt A, Valbusa G, et al. E-3810 is a potent dual inhibitor of VEGFR and FGFR that exerts antitumor activity in multiple preclinical models. Cancer Res 2011;71:1396–405.
28. Soria J-C, DeBraud F, Bahleda R, Adamo B, Andre F, Dientsmann R, et al. Phase I/IIa study evaluating the safety, efficacy, pharmacokinetics, and pharmacodynamics of lucitanib in advanced solid tumors. Ann Oncol 2014;25:2244–51.
29. Chen C, Liu Y, Liu Y, Zheng P. mTOR regulation and therapeutic rejuvenation of aging hematopoietic stem cells. Sci Signal 2009;2:ra75.
30. Stuhlmiller Timothy J, Miller Samantha M, Zawistowski Jon S, Nakamura K, Beltran Adriana S, Duncan James S, et al. Inhibition of lapatinib-induced kinome reprogramming in ERBB2-positive breast cancer by targeting BET family bromodomains. Cell Rep 2015;11:390–404.
31. Johnston O, Rose CL, Webster AC, Gill JS. Sirolimus is associated with new-onset diabetes in kidney transplant recipients. J Am Soc Nephrol 2008;19: 1411–8.
32. Hamanaka RB, Glasauer A, Hoover P, Yang S, Blatt H, Mullen AR, et al. Mitochondrial reactive oxygen species promote epidermal differentiation and hair follicle development. Sci Signal 2013;6:ra8.
33. Wilson TR, Fridlyand J, Yan Y, Penuel E, Burton L, Chan E, et al. Widespread potential for growth-factor-driven resistance to anticancer kinase inhibitors. Nature 2012;487:505–9.
34. Hitosugi T, Fan J, Chung T-W, Lythgoe K, Wang X, Xie J, et al. Tyrosine phosphorylation of mitochondrial pyruvate dehydrogenase kinase 1 is important for cancer metabolism. Mol Cell 2011;44:864–77.
35. Chioni A-M, Grose R. FGFR1 cleavage and nuclear translocation regulates breast cancer cell behavior. J Cell Biol 2012;197:801–17.
36. Charafe-Jauffret E, Ginestier C, Iovino F, Wicinski J, Cervera N, Finetti P, et al. Breast cancer cell lines contain functional cancer stem cells with metastatic capacity and a distinct molecular signature. Cancer Res 2009;69:1302–13.
37. Chaffer CL, Marjanovic ND, Lee T, Bell G, Kleer CG, Reinhardt F, et al. Poised chromatin at the ZEB1 promoter enables cell plasticity and enhances tumorigenicity. Cell 2013;154:61–74.
38. Hwang-Verslues WW, Kuo W-H, Chang P-H, Pan C-C, Wang H-H, Tsai S-T, et al. Multiple lineages of human breast cancer stem/progenitor cells identified by profiling with stem cell markers. PLoS One 2009;4:e8377.
39. Yoon C-H, Kim M-J, Lee H, Kim R-K, Lim E-J, Yoo K-C, et al. PTTG1 oncogene promotes tumor malignancy via epithelial to mesenchymal transition and expansion of cancer stem cell population. J Biol Chem 2012;287:19516–27.
40. Lang J-Y, Hsu Jennifer L, Meric-Bernstam F, Chang C-J, Wang Q, Bao Y, et al. BikDD eliminates breast cancer initiating cells and synergizes with lapatinib for breast cancer treatment. Cancer Cell 2011;20:341–56.
41. Silva IA, Bai S, McLean K, Yang K, Griffith K, Thomas D, et al. Aldehyde dehydrogenase in combination with CD133 defines angiogenic ovarian cancer stem cells that portend poor patient survival. Cancer Res 2011;71: 3991–4001.